3.2.5

In-situ structural integrity evaluation for high-power pulsed spallation neutron source by using a laser Doppler method

T. Wan, T. Naoe, T. Wakui, K. Haga, H. Kogawa and M. Futakawa

J-PARC Center, 2-4 Shirane Shirakata, Tokai-mura, Ibaraki 319-1195, Japan

wan.tao@jaea.go.jp

Abstract. High-power pulsed spallation neutron sources are being developed in the world. Mercury is used as a target material to produce neutrons. At the moment of the proton beams bombard the mercury target, the mercury target vessel is impulsively excited resulting from the interaction between mercury and solid wall due to the pressure waves. The vibrational velocity on the outer surface of the target vessel was measured by a laser Doppler vibrometer to diagnose the structural integrity of the vessel. Measured vibrational signals, were applied for evaluating the damage inside the target vessel that is induced by the cyclic loading and cavitation bubble collapsing due to the pressure waves. A technique, the Wavelet Differential Analysis (WDA), was applied to clearly indicate the effects of damages on the impulsive vibration behavior. Moreover, in order to reduce the effects of superimposed noise on the vibration signals on the WDA, the statistical methods, the Analysis of Variance (ANOVA) and the Analysis of Covariance (ANCOVA), were applied. The lab-experimental results, numerical simulation results with manually added random noise, and field data were analysed by the statistic methods. The results demonstrated that the established in-situ diagnostic technique can effectively evaluate the structural integrity.

Nomenclature

WDA	Wavelet Differential Analysis	
WDI	Wavelet Differential Image	
Img	Wavelet Image	
f	frequency	Hz
t	time	s
I_a	average intensity of WDI	
D	diameter of damage	mm
$V(t,f)$	value of intensity of the WDI at time t and frequency f	dB
SS_T	total sum of square	
n	total number of samples	
y_{ij}	*jth* sample value of the *ith* group	
M	sample mean of all samples	
h	number of samples in each group	
$\bar{y}_i$	sample mean of the *ith* group	

X	factor X that affects the vibration behavior
Y	factor Y that affects the vibration behavior
SS_b	sum of square between groups of samples
SS_e	sum of square within groups of samples
SS_X	sum of square due to factor X
SS_Y	sum of square due to factor Y
D_X	degree of freedom of factor X
D_e	degree of freedom of within groups of samples
F	calculation value of F-test
SS_{noise}	sum of square due to noise
$SS_{residual}$	sum of square excluding noise
$D_{e'}$	degree of freedom of modified within groups of samples
$SS_{b'}$	modified sum of square between groups of samples
$SS_{e'}$	modified sum of square within groups of samples
F'	modified calculation value of F-test
T	calculation value of t-test
$\bar{y}_k$, $\bar{y}_l$	modified sample mean of the *kth* and *lth* group
$S_{\bar{y}_k - \bar{y}_l}$	standard error of the modified sample mean
$f(x)$	random function of noise amplitude
A,-A	maximum amplitude value of noise
c, d	constants

1. Introduction

High-power pulsed spallation neutron sources are being developed in the world. In the Japan Spallation Neutron Source (JSNS), pulsed proton beams (25 Hz, 1 μs pulse duration) are injected into a mercury target to produce neutrons for the innovative materials and life science research. The mercury target vessel is a triple walled structure consisted of water shroud, helium vessel, and mercury vessel. The proton beam window of mercury vessel has a double-walled structure consists of inner and outer walls with a mercury narrow channel. However, various kinds of damages, such as cavitation, cyclic fatigue and proton and neutron irradiation damage, are imposed on the target vessel during its operation. Especially the cavitation damage caused by the pressure waves is a critical issue for the target vessel. Pressure waves are generated in the mercury due to rapid heat deposition resulting from the proton beam injection [1, 2]. The pressure waves propagate to the target vessel and impose cavitation damage on the inner wall, especially at the beam window portion [3]. Meanwhile, the pressure waves give rise to the vibration of the target vessel.

The cavitation damage remarkably reduces the life-time of the target vessel [4, 5]. To solve this issue, the micro bubbles injection technique is being developed by Japan Atomic Energy Agency (JAEA) to mitigate the pressure waves [6~11]. On the other hand, it is also important to establish the structure integrity evaluation technique for the target vessel, which is strongly expected from the viewpoint of estimating the lifetime of the target and keeping stable operation.

The dynamic responses of the target vessel vibration caused by the pressure waves were focused on to develop the structure integrity evaluation technique. A laser Doppler vibrometer (LDV) was installed as an in-situ diagnostic system with the advantage of providing an entirely remote and non-contact technique, which prevents the sensor from the radiation damage [12]. This diagnostic technique can be applied to the structural integrity diagnosis for not only the nuclear facilities but also extreme environments where a human activity is extremely limited, such as in the space and the oceans.

In the case of numerous cavitation damage imposed on the inner wall of the target vessel, the vessel might be easily deformed by the thermal stress because the thickness of wall is reduced, and the gap of the window channel would be possibly reduced due to the deformation. The cavitation damage is accumulated on the inner wall and if it was severe enough, the inner wall would be broken and a

penetrated damage would be formed on it. The vibration signals will be affected by the deformation of inner wall and the penetrated cavitation damage, as shown in Fig.1.

In a previous study, penetrated cavitation damage was assumed on the inner wall of target vessel [13]. The dependency of dynamic responses of double-walled target vessel on cavitation damage was investigated through the numerical simulation. The diagnostic technique, Wavelet Differential Analysis (WDA), was developed to clearly observe the differences of vibration signals that are dependent on cavitation damage.

Nevertheless, the damage dependency is usually covered by the noise that appears in the lab-scale experimental and real system of field data which was obtained by the LDV during the operation of the real target. In the present study, on basis of the WDA technique, the statistical methods referred to as Analysis of Variance (ANOVA) and Analysis of Covariance (ANCOVA) were used to reduce the noise effect on the impulsive vibration behavior.

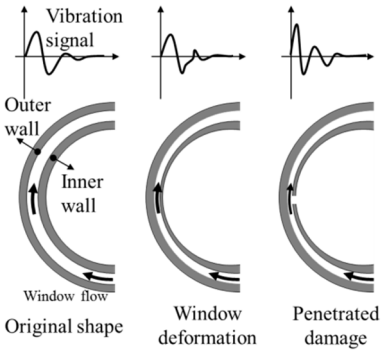

Figure 1. Schematic drawing of window deformation, damage scenarios and target vessel vibration.

2. Experiments

To experimentally investigate the dependency of vibration behavior on damage, an electro-Magnetic IMpact Testing Machine (MIMTM) was used to simulate the double-walled structure of the target vessel. Figure 2 shows the schematic of detection setup of MIMTM vibration. An electro-magnetically driven striker impulsively impacted the mercury, which was filled in a chamber with a size of Φ100×15 mm^3, to impose the pressure waves on type 316L stainless steel plate specimen (60×60×2.5t mm^3), which is the same material as the mercury vessel was fixed into the chamber by bolts. The gap between the specimen and the upper wall of MIMTM was fixed to 2.3 mm. In order to moderate the penetrated cavitation damage on the inner wall, penetrated holes with diameters of 1, 2, 5, and 10 mm were made at the center of the specimens, respectively. Impulsive pressure signals were induced in mercury at a power of 560W/pulse with a repetition rate of 1 Hz. The cavitation damage occurred under such a condition in the MIMTM was roughly similar to that of the MW-class proton beam injection [14].

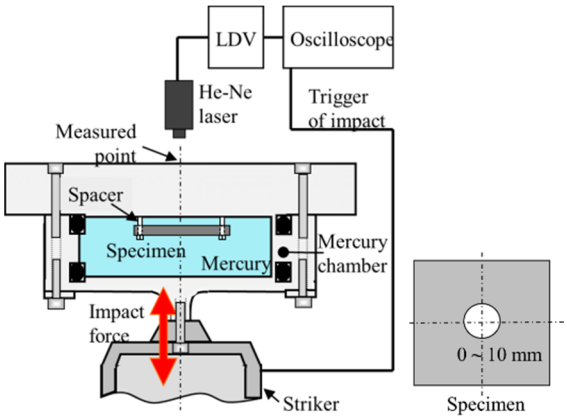

Figure 2. Schematic drawing of measuring system of MIMTM vibration.

The vibration of MIMTM was subsequently detected by a He-Ne laser Doppler vibrometer (Onosokki, LV1710). The laser (wavelength: 633 nm) was illuminated onto the center of the upper rid of the mercury chamber. The detectable frequency range was from 1 Hz to 3 MHz with a sensitivity of 0.01 (m/s)/v. The detected vibration velocity signals were saved in an oscilloscope with a sampling rate of 1.25 MHz. The oscilloscope was triggered by the drive signal of the electromagnetic coil. Each signal was obtained by averaging 100 impacts in order to reduce the background noise.

3. Numerical simulations

In order to investigate the dependency of dynamic responses of the double-walled target vessel on damage under conditions of various proton beam powers, FEM analyses were carried out using a conventional code LS-DYNA [13, 15]. A half model (Figure 3) for the double-walled target vessel of JSNS was established. The gap between the outer and the inner walls was set 2 mm. Structures and the mercury were meshed as a half model by the shell and solid elements, respectively. Numbers of shell and solid elements were 95052 and 1758852, respectively. The boundary of Z-direction of the bottom of the vessel was kept fixed, and that of the end of the mercury was set to be non-reflecting.

Penetrated damage holes with diameters of 1, 5, 10, 20 and 40 mm were assumed on the inner wall of the target vessel at the center of the beam incident area, as shown in Figure 4. This position is most likely to be damaged [3]. The output node position, measuring point, is the same as the LDV measurement point on the real target vessel. In this simulation, helium vessel and water shroud was ignored, because the effects of helium vessel and water shroud on vibration signals have been checked and the results are unremarkable.

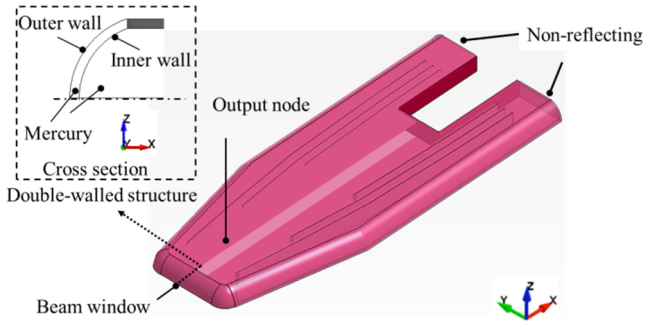

Figure 3. Geometrical model of mercury vessel.

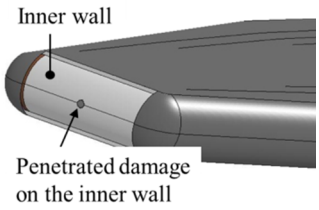

Figure 4. Damage location.

4. Analysis methods and calculation procedure

4.1. Wavelet differential analysis [13]

In order to clearly and quantitatively indicate the differences caused by damage, first, the wavelet differential process for the time responses of vibration velocity was carried out; the process is described by Eq. (1):

$$WDI_D = |Img_D - Img_0| \,/\, |Img_0| \,, \tag{1}$$

where *WDI* is the wavelet differential image, *Img* is the wavelet image of vibration signal, and the subscripts *D* represents the damage with a diameter of *D* mm, whereas the subscript *0* implies no damage. Then, the average intensity (I_a) of the wavelet differential image (*WDI*) could be calculated through equations (2) – (4).

$$I_a = \int^{\Delta f} \int^{\Delta t} V(t,f)dtdf \,, \tag{2}$$

$$\Delta f = f_2 - f_1 \,, \tag{3}$$

$$\Delta t = t_2 - t_1 \,, \tag{4}$$

where measuring frequency ranges from f_1 to f_2 (in hertz), and measuring time ranges from t_1 to t_2 (in seconds); $V(t, f)$ is the value of the intensity of the WDI at time t and frequency f (in decibels), and I_a is the average intensity of the differential image.

4.2. Applied statistical methods

4.2.1. *Analysis of variance* In the present study, we are very interested in the differences of vibrational signals caused by damage. In order to analyse the differences of groups of WDI results, the statistic method referred to as the ANOVA was applied. In ANOVA, the total variation of data is portioned into several components [16-18]. The total variation of the system, defined by the total sum of squares term, SS_T:

$$SS_T = \sum_{ij}(y_{ij} - M)^2 \quad for\, i, j = 1, 2, 3, \cdots, p, \tag{5}$$

$$M = \frac{1}{n}\sum y_{ij} \ , \tag{6}$$

where n represents the total number of samples; y_{ij} represents the jth sample value in the ith group; M is the sample mean of all samples.

Experimental studies contain certain test error, and so it is necessary to calculate the error variance in ANOVA. The total sum of square can be divided into the sum of square between groups of samples, SS_b, and sum of square within groups of samples (caused by error), SS_e:

$$SS_T = SS_b + SS_e \ , \tag{7}$$

$$SS_b = \sum_i h(\bar{y}_i - M)^2 \ , \tag{8}$$

$$SS_e = \sum_{ij}(y_{ij} - \bar{y}_i)^2 \ , \tag{9}$$

where h is the number of samples in each group, $\bar{y}_i$ is the sample mean of the ith group.

If there are two main factors that affect the results and the two factors have no mutual interactions with each other, then the total sum of square can be expressed as:

$$SS_T = SS_X + SS_Y + SS_e \ , \tag{10}$$

where SS_X and SS_Y represent variations due to factor X and Y, respectively.

Degrees of freedom need also to be considered together with each sum of squares whilst performing ANOVA calculations. Subsequently, the obtained data are used to calculate the value F of F-test. The value of F for factor X can be expressed as following:

$$F = \frac{SS_X/D_X}{SS_e/D_e} \ , \tag{11}$$

where D_X and D_e are the degree of freedom of factor X and within groups of samples, respectively. The value of F for factor Y can be calculated as the same way.

The value F represents the difference degree between the groups of samples. Larger F value means there are more obvious differences between groups of samples.

4.2.2. *Analysis of covariance* ANCOVA is a statistic method that combined regression and ANOVA [16]. When the noise level is considerable high, it might have significant effects on the vibration analysis. The damage dependency might be masked by the noise. So it is necessary to remove the noise effects from the results. In ANCOVA, the total sum of square, SS_T, can be divided into the sum of square of noise, SS_{noise}, and that of excluding noise, $SS_{residual}$, which is shown as:

$$SS_T = SS_{noise} + SS_{residual} \ , \tag{12}$$

The former part at the right hand of the equation can be removed by a regression analysis. The sample mean of each group is modified by the regression. The sum of square of residual part consists

of modified sum of square between groups of samples, $SS_{b\prime}$, and modified sum of square within one group of samples, $SS_{e\prime}$. It can be expressed that:

$$SS_{residual} = SS_{b\prime} + SS_{e\prime}, \tag{13}$$

Subsequently, F-test was carried out (taking factor X as an example):

$$F' = \frac{SS_{b\prime}/D_X}{SS_{e\prime}/D_{e\prime}}, \tag{14}$$

where $D_{e\prime}$ represents the degree of freedoms of modified within groups of samples. The F' factor is considered to be able of indicating the differences more exactly because the noise effect is taken into consideration.

Finally, t-test was carried out for multiple comparisons between the modified groups of samples. It can be expressed as the following:

$$T = \frac{\bar{y}_k - \bar{y}_l}{S_{\bar{y}_k - \bar{y}_l}}, \tag{15}$$

where $\bar{y}_k$ and $\bar{y}_l$ are the modified sample mean of the *kth* and *lth* group; $S_{\bar{y}_k - \bar{y}_l}$ is the standard error of the modified sample mean. Similar with the *F* factor, the *T* value represents the difference degree between the groups of data.

4.3. Calculation procedure

In order to reduce the noise effects on the results, the WDA, ANOVA and ANCOVA were applied to raw data analysis, by the following calculation procedure.

Many parameters, such as damage size, beam power, bubble condition, etc., may impose effects on the target vessel vibration results. At first we are very interested in the damage size effects on the vibration behaviours of target vessel. In the following text of this sub-section, damage size is selected as the parameter to introduce the calculation procedure under the condition of fixing other parameters.

Figure 5 shows the flow chart of calculation procedure. First, one reference raw data should be selected, which is usually the time response of vibration signals with minimum damage among the raw data which needed to be analysed. The raw data should be classified into different groups, and each group represents one level of damage degree. The number of samples in one group, *h*, is the same in each group. Subsequently the wavelet differential images were obtained between the data in each group and the reference data, and then the I_a of each *WDI* was calculated. Through the above calculations, I_a of *WDIs* was got in each group with a number of *h*. The simple average value and error bar for the I_a of *WDIs* in each group can be calculated. After that, group number one that with the minimum damage is set as the reference group. The ANOVA and ANCOVA are carried out by using I_a of *WDIs* between other groups and group number one, respectively. The *F* factor of ANOVA and *T* factor of the ANCOVA can be obtained to indicate the degree of difference between other groups and group number one. Larger value of *F* or *T* indicates more significant differences between groups.

5. Results and discussions

5.1. MIMTM vibration

Figure 6 shows the time responses of MIMTM vibration velocity. It can be seen that the differences between the dynamic responses without damage and that with damage is obvious. To quantify the penetrated damage size dependency, the I_a *of WDI* was calculated. Figure 7 shows the I_a *of WDI* as a function of the damage size. The average vale of I_a *of WDI* is dependent on the damage size, however, the tendency of I_a *of WDI* is unobvious, and error bar is large for each group of twelve data. This is because experimental results contain noise and the I_a of *WDI* is sensitive to noise. Therefore, the dependency of I_a of *WDI* on damage is influenced by noise. Subsequently ANOVA was carried out. The data was grouped by damage size. The noise in each data is different. The group of data without

damage was set as the reference group. Figure 8 shows normalized *F* factor of ANOVA as a function of the penetrated damage size. The damage dependency is clearly recognized by using *F* factor of ANOVA. The *F* factor increases steadily when the damage size trends larger. The differences between the time responses of vibration velocity with damage and those without damage trend much more obvious with increasing the damage size. From the results, it is learned that larger damage size imposes more significant effects on the vessel vibration. If a penetrating damage forms on the inner wall of the target vessel, pressure waves propagate through the damage to vibrate the outer wall of target vessel. When the damage trends larger, more energy will be carried by the waves to impact the outer wall, and thus stronger vibration of the target vessel is aroused.

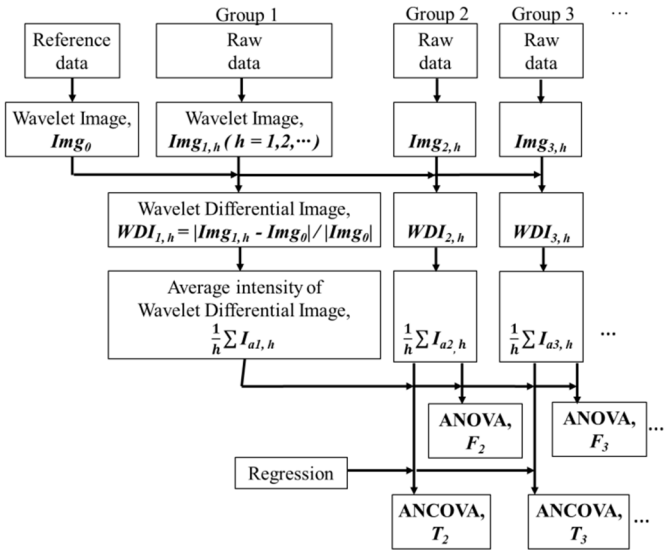

Figure 5. Flow chart of calculation procedure.

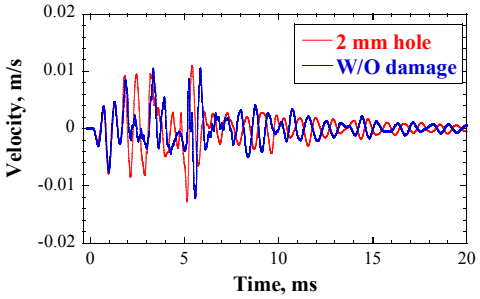

Figure 6. Time responses of vibration velocity of MIMTM.

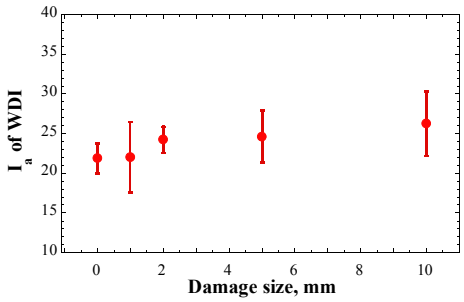

Figure 7. Average intensity of wavelet differential image as a function of damage size of penetrated cavitation damage for MIMTM vibration.

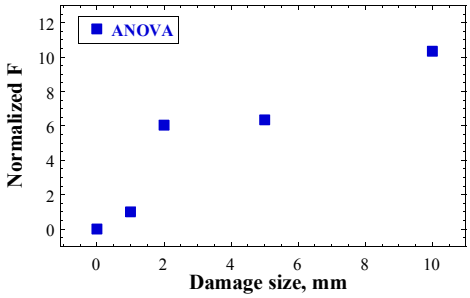

Figure 8. Normalized F factor of ANOVA as a function of the size of penetrated cavitation damage.

5.2. Target vessel vibration

5.2.1. *Beam power: 1MW* The size of target vessel is much larger than that of MIMTM, and thus the frequency components of the time responses of vibration are different. Besides the MIMTM study, the target vessel vibration also should be investigated. The damage size was controlled in the numerical simulations, and the numerical simulation results were used to analyse the dependency of target vessel vibration on damage. Random noise was manually added into the vibration signals that obtained by the

numerical simulations. The evaluation procedure was then applied to such vibration signals with noise. The noise was added by a random function that can be expressed as:

$$f(x) \in (-A, A), \tag{16}$$

where A represents the maximum amplitude of the noise and can be selected manually. Noise with amplitude $|A|$ could be added to the vibration signals by using this random function. For each damage condition, twelve data were obtained by adding the random noise.

Firstly, noise with maximum amplitude of about 7% of the maximum vibration velocity amplitude, was added to the numerical simulation signals (beam power: 1 MW). Figure 9 shows an example of time responses of vibration velocity for target vessel and the corresponding wavelet images before and after adding the noise. The wavelet image was significantly changed after adding the noise, especially in the relatively higher frequency range. The average value of I_a of *WDI* as a function of the penetrated damage size was shown in Figure 10. The absolute value of error bar is similar with the MIMTM case. Obviously, compared with results obtained by the numerical simulation [13], the added noise changed the value of I_a of *WDI* and induced large error bar. However, though the dependency of I_a of *WDI* on damage size was unobvious, the trend was not changed by the noise. Figure 11 shows the normalized F factor of ANOVA as a function of the penetrated damage size. By applying the ANOVA, the damage dependency was enhanced. It illustrates that ANOVA is effective to enhance the effect of damage on vibration signals for the low noise level.

When the noise level is not strong enough to change the trend of damage dependency, the effects of noise on the vibrational signals is not significant and can be reduced through applying ANOVA for analysing the I_a of *WDIs*.

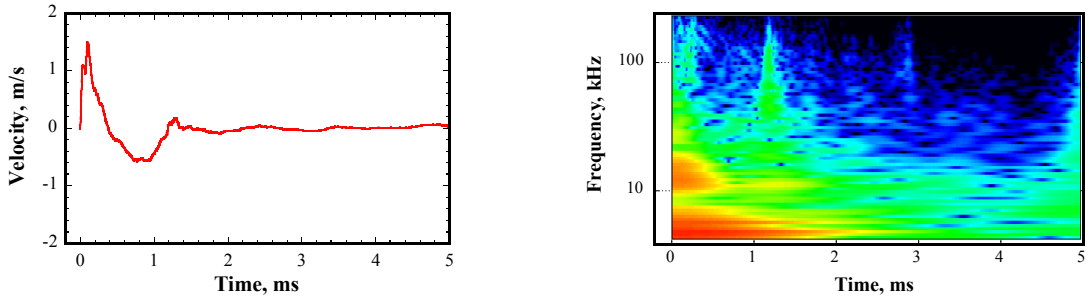

(a) Numerical simulation signals [13]; 1 MW, without damage

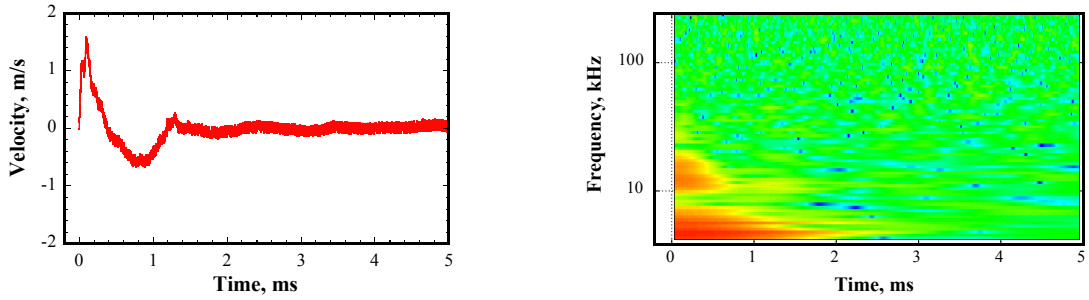

(b) Add 7% noise to the numerical simulation signals

Figure 9. Time responses of vibration velocity for target vessel and the corresponding wavelet images; numerical simulation and add 7% noise.

5.2.2. *Beam power: 100 kW* Figure 12 shows one vibration signal obtained from the real target. The proton beam power is 100 kW. Strong noise could be viewed in the vibration signal. To investigate the damage dependency under such a beam power condition, numerical simulations were carried out. Average intensity of wavelet differential image was plotted as a function of the damage size, as shown in Figure 13. Independent of the beam power, the average intensity of wavelet differential image is

proportional to the damage size. The comparative increments of energy, which is carried by the waves that penetrate the damage hole to excite the outer wall of target vessel, trends larger when the damage size becomes larger.

Figure 14(a) shows an example of vibration signal obtained by the numerical simulation. The beam power is 100 kW without damage. To simulate the noise level of the field data, the maximum amplitude of added noise was increased to about 30% of the maximum amplitude of the vibration signal. Figure 14(b) shows the vibration signal with manually added noise. The noise level is comparable to the field data that obtained from the real target. Then such vibration signals with manually added noise were used for the analysis.

Figure 15 shows the average value of I_a of *WDI*, *F* factor of ANOVA and *T* factor of ANCOVA as a function of the penetrated cavitation damage size. The error bar of I_a of *WDI* becomes much larger relative to the lower noise situation due to a much stronger noise level. The trend of damage dependency changes due to the strong noise level. In this case, the *F* factor of ANOVA fails to indicate the damage size dependency due to the strong noise. Therefore, the noise effects should be taken into consideration and be moved. Thereafter, the ANCOVA was applied to analyse the data. The dependency of *T* factor on damage size can be fairly observed. ANCOVA effectively reveals the damage dependency even in case of a strong noise level.

Figure 16 shows the damage size as a function of normalized *T* factor for the experimental and numerical simulation results. The trends showed by the experimental and numerical simulation results are similar with each other, which is coincidence with the variation trend showed in Figure 13. The correlation between damage size and *T* factor could be given by:

$$D = c \times T^d \,, \tag{17}$$

where *D* is the size of penetrated damage, unit is mm; *c, d* are constants related to the material property, structure geometry, etc.

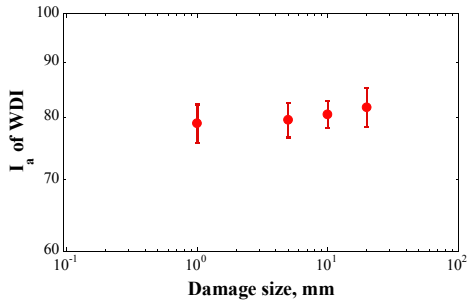

Figure 10. Average intensity of wavelet differential images as a function of the size of penetrated cavitation damage; add 7% noise to the numerical simulation signals.

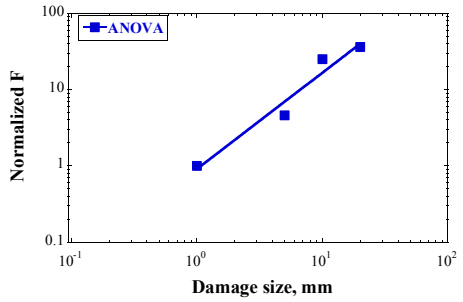

Figure 11. Normalized F factor of ANOVA as a function of the size of penetrated cavitation damage; add 7% noise to the numerical simulation signals.

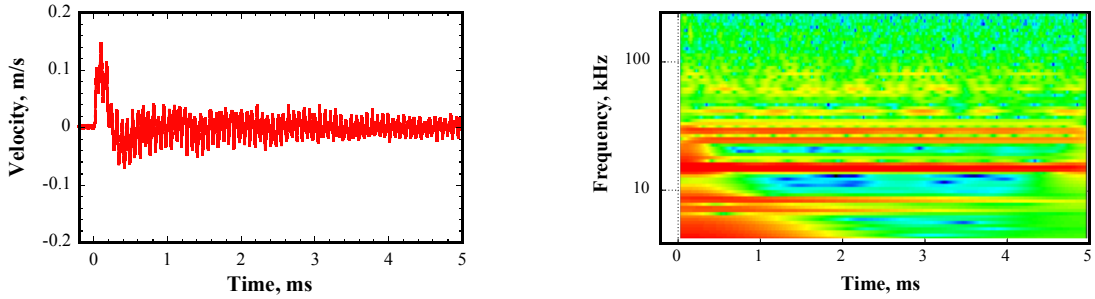

Figure 12. Field data obtained from the real target and the corresponding wavelet image; beam power: 100 kW.

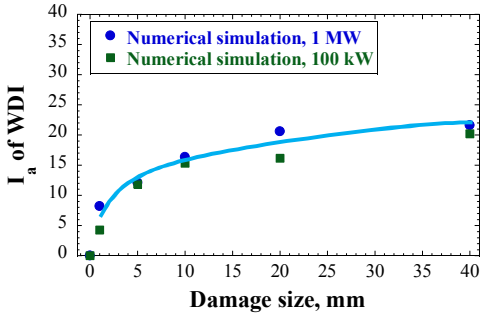

Figure 13. Average intensity of wavelet differential image as a function of damage size.

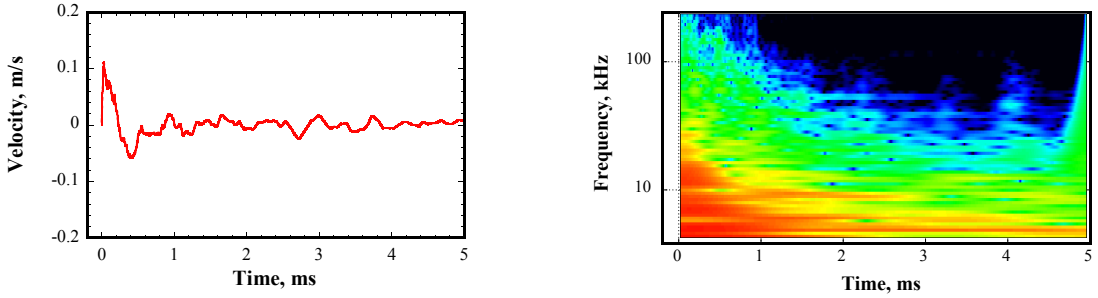

(a) Numerical simulation signal and the corresponding wavelet image; 100 kW, without damage

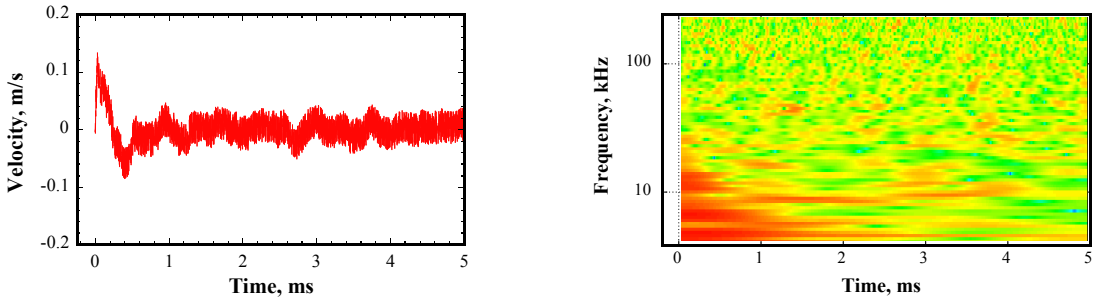

(b) Add 30% noise to the numerical simulation signal and the corresponding wavelet image

Figure 14. Time responses of vibration velocity for target vessel and the corresponding wavelet images; numerical simulation and add 30% noise.

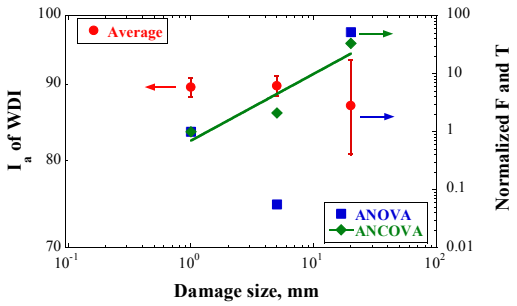

Figure 15. I_a of WDI, normalized F of ANOVA, and normalized T of ANCOVA as a function of the penetrated cavitation damage size; add 30% noise to the numerical simulation signals.

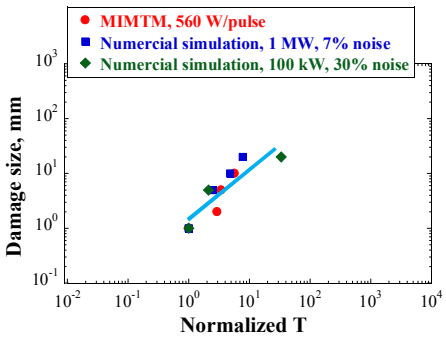

Figure 16. Damage size as a function of the normalized T factor.

5.3. Field application

As introduced previously, in the JSNS mercury target, Helium gas is injected into the target vessel to form micro-bubbles in mercury to mitigate the pressure waves [7]. The microbubbles-induced void fraction in the mercury is controlled by the flow rate of gas injection. The vibration behavior of the target vessel is closely related to the void fraction of liquid mercury [8]. ANCOVA was applied for analyzing the vibration signals obtained from the real target with various flow rate of gas injection.

The vibration signals were acquired from the real target at a certain time in several different days. The beam power and damage degree during the data acquisition period could be considered the same. Figure 17 shows an example of field data detected from the real target. The noise level is considerably high. The corresponding noise signal was obtained by each field vibration signal minus the averaged vibration signal of one day. Figure 18 shows the I_a and T factor as a function of the data acquisition date. The I_a fluctuates slightly, whereas the T factor firstly increases quickly and then fluctuates slightly. It is considered that the variation trend of T factor is related to the absolute differential He flow rate. To check this, the absolute differential He flow rate and normalized T factor was plotted as a function of the data acquisition date, as shown in Figure 19. Obviously, the variation trend of the absolute differential flow rate and normalized T factor fits well to each other. ANCOVA effectively reduced the effect of noise and revealed the gas flow rate dependency.

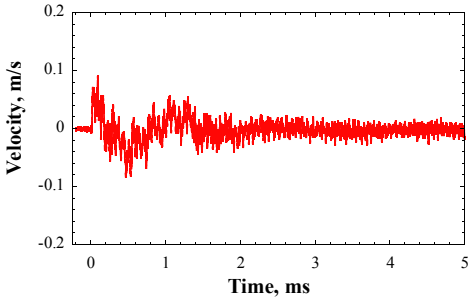

Figure 17. Field data obtained from the real target; with micro bubbles injection.

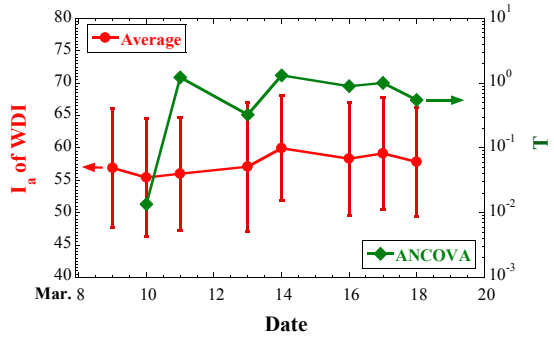

Figure 18. I_a of WDI and T factor of ANCOVA as a function of data acquisition date.

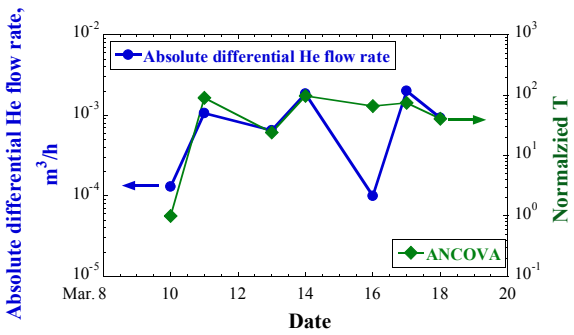

Figure 19. Absolute differential He flow rate and normalized T factor of ANCOVA as a function of data acquisition date.

6. Conclusion

A laser Doppler vibrometer method for monitoring the target vessel vibration was employed to establish the in-situ structure integrity evaluation technique for the JSNS mercury target:

1) Wavelet Differential Analysis (WDA) technique was developed to enhance the differences between vibrational signals. The vibration behavior of target vessel is very dependent on the damage size.
2) Analysis of covariance (ANCOVA) was applied to reduce the noise effects on the vibrational signals, and the T factor of ANCOVA clearly indicated the damage dependency on the vibrational

signals.

3) The combination of the WDA and ANCOVA could be possibly used to evaluate other parameters that are related to the structural vibration.

The established in-situ diagnostic technique proposes a possible way for in noncontact and remotely structure integrity evaluation.

Acknowledgement

This work was partly supported by the Japan Society for the Promotion of Science through a Grant-in-Aid for Scientific Research C (No. 23360088).

References

[1] Futakawa M, Kogawa H, Hino R 2000 *J. Phys. VI France* **10** 237.
[2] Futakawa M, Kikuchi K, Conrad H, Stechemesser H 2000 *Nucl. Instrum. Meth. A* **439** 1.
[3] McClintock D A, Riemer B W, Ferguson P D, Carroll A J, Dayton M J 2012 *J. Nucl. Mater.* **431** 147.
[4] Futakawa M, Kogawa H, Hasegawa S, Ikeda Y, Riemer B, Wendel M, Haines J, Naoe T, Tanaka N, Okita K, Fujiwara A, Matsumoto Y 2006 *Sixth International Symposium on Cavitation* 1.
[5] Futakawa M, Kogawa H, Hasegawa S, Ikeda Y, Riemer B, Wendel M, Haines J, Bauer G, Naoe T, Okita K, Fujiwara A, Matsumoto Y, Tanaka N 2008 *J. Nucl. Mater* **377** 182.
[6] Kogawa H, Shobu T, Futakawa M, Bucheeri A, Haga K, Naoe T 2008 *J. Nucl. Mater* **377** 189.
[7] Futakawa M, Kogawa H, Hasegawa S, Naoe T, Ida M, Haga K, Wakui T, Tanaka N, Matsumoto Yand Ikeda Y 2008 *J. Nucl. Sci. Technol.* **45** 1041.
[8] Naoe T, Kogawa H, Futakawa M, Ida M 2011 *J. Nucl. Sci. Technol.* **48** 865.
[9] Naoe T, Ida M, Futakwa M 2008 *Nucl. Instrum. Meth. A* **586** 382.
[10] Naoe T, Hasegawa S, Bucheeri A, Futakawa M 2008 *J. Nucl. Sci. Technol.* **45** 1233.
[11] Riemer B W, Wendel M W, Felde D K, Abdou A A, McClintock D A 2012 *J. Nucl. Mater.* **431** 160.
[12] Teshigawara M, Wakui T, Naoe T, Kogawa H, Maekawa F, Futakawa M, Kikuchi K 2010 *J. Nucl. Mater.* **398** 238.
[13] Wan T, Wakui T, Naoe T, Futakawa M, Maekawa K 2014 *Appl. Mech. Mater.* **566** 629.
[14] Futakawa M, Naoe T, Kogawa H, Tsai C C, Ikeda Y 2003 *J. Nucl. Sci. Technol.* **40** 895.
[15] Hallquist J O 2006 *LS-DYNA Theory Manual* (USA: Livermore Software Technology Corporation).
[16] Rutherford A 2012 *Introducing Anova and Ancova: A GLM Approach* (Hoboken John: Wiley & Sons, Inc.).
[17] Gopalsamy B M, Mondal B, Ghosh S 2009 *Int. J.Adv. Manuf. Tech.* **45** 1068.
[18] Zahid A K, Arshad N S 2012 *Int. J.Mater. Prod. Tec.* **43** 2.